Energy Reports 6 (2020) 721–733

Contents lists available at ScienceDirect

Energy Reports

journal homepage: www.elsevier.com/locate/egyr

Research paper

Hydrocarbon migration and accumulation in the Lower Cambrian to Neoproterozoic reservoirs in the Micangshan tectonic zone, China: New evidence of fluid inclusions

Tao Tian [a,b], Peng Yang [c,*], Zhanli Ren [c,**], Deliang Fu [a], Shixin Zhou [d], Fu Yang [a], Jing Li [d]

[a] Key Laboratory of Coal Resources Exploration and Comprehensive Utilization, Ministry of Natural Resources, Xián 710021, China
[b] Shandong Key Laboratory of Depositional Mineralization & Sedimentary Minerals, Shandong University of Science and Technology, Qingdao 266590, China
[c] State Key Laboratory of Continental Dynamics, Department of Geology, Northwest University, Xi'an 710069, China
[d] Lanzhou Center for Oil and Gas Resources, Institute of Geology and Geophysics, Chinese Academy of Sciences, Lanzhou 73000, China

ARTICLE INFO

Article history:
Received 19 September 2019
Received in revised form 10 January 2020
Accepted 10 March 2020
Available online xxxx

Keywords:
Fluid inclusion
Hydrocarbon charge history
Petroleum systems
Niutitang Formation
Micangshan tectonic zone

ABSTRACT

The Lower Paleozoic reservoir in the Micangshan tectonic zone is a new shale gas exploration area with excellent potential. However, the hydrocarbon migration and accumulation histories of this reservoir have not been thoroughly elucidated and urgently require further research. Fluid inclusions offer a unique and useful method to test for hydrocarbon migration, accumulation, composition and timing. This study integrated the hydrocarbon charge history using fluid inclusions in the Lower Cambrian to Neoproterozoic reservoir from the Micangshan tectonic zone. This work involves the delineation and analysis of fluid inclusions using the petrography, spectroscopy and microthermometry of fluid inclusions. Based on the fluid inclusion analyses combined with reservoir thermal history, timing estimates and charge models of the hydrocarbons were obtained. The formation of natural gas was multifactorial in the Lower Cambrian to Neoproterozoic petroleum system, and the gas in the Niutitang ($\epsilon_1 n$) and Dengying ($Z_2 d$) reservoirs was mainly from oil cracking and dry gas, and gas in the Xiannvdong ($\epsilon_1 x$) and Canglangpu ($\epsilon_1 c$) reservoirs was abiogenic and formed in hydrothermal fluids by regional tectonothermal events. Three well-defined stages of hydrocarbon charge were identified in the petroleum system in the Micangshan tectonic zone. The stage of oil charge first began before the Early Permian (~277 Ma); the stage of gas charge from oil cracking occurred in the Late Triassic to Early Jurassic (212 Ma-198 Ma); and the stage of gas charge from dry gas occurred in the Middle Jurassic (173 Ma-166 Ma). The gas of mixed origin from the Niutitang reservoir was stored in the nanoscale pores as a self-reservoir, rather than as an effective gas source for the overlying reservoirs.

1. Introduction

Considerable shale gas and natural gas exploration and development work has been completed in South China, and previous work suggests that the Lower Cambrian to Neoproterozoic gas reservoirs played an important role in gas production in the Sichuan Basin and its peripheral regions (Dong et al., 2016; Gao et al., 2015; Huang et al., 2012; Liu et al., 2013; Xi et al., 2016; Zou et al., 2015, 2016). The Micangshan tectonic zone is in the transitional area between the Sichuan Basin and the Qinling Orogenic Belt, whose distinctive geological conditions are more complex than those in the Sichuan Basin (Xu et al., 2009). In recent years, commercial volumes of shale gas have been found in the Niutitang Formation ($\epsilon_1 n$), and the latest research suggests that the Lower Cambrian and Neopoterozoic in the Micangshan tectonic zone may contain new and ideal exploration target reservoirs (Fu et al., 2018; Tian et al., 2019a,b). Understanding the hydrocarbon migration and accumulation histories of the above two reservoirs are of great significance for guiding future shale gas and natural gas exploration in the Micangshan tectonic zone.

Fluid inclusions are entrapped during primary mineral growth, as well as during the healing of later microfractures, which can provide accurate information on the pressure and temperature of mineral growth and the of fluids compositions involved in diagenesis (Barona et al., 2008; Bhattacharya et al., 2014; Dolson, 2016). In particular, hydrocarbons entrapped within fluid inclusions can provide conclusive evidence that hydrocarbons migrated and accumulated in the rock (Barona et al., 2008).

* Correspondence to: Department of Geology Northwest University, Taibai Road No.229, Beilin, Xián, 710069, China.
** Corresponding author.
E-mail addresses: p.yang@nwu.edu.cn, 13909263435@163.com (P. Yang), renzhanl@nwu.edu.cn (Z. Ren).

https://doi.org/10.1016/j.egyr.2020.03.012

Placing the occurrence of hydrocarbon fluid inclusions in a paragenetic sequence allows relative dating of hydrocarbon migration in relation to reservoir diagenesis and tectonic events (Jensensuis and Burruss, 1990). Parnell (2010) discussed the importance of fluid inclusions in assessing the burial history of a petroleum system in terms of the timing of oil migration, the occurrence and distribution of different pulses of oil migration and reservoir compartmentalization. Fluid inclusions have become one of the most important tools for investigating the histories of hydrocarbon migrations and accumulations (George et al., 2004; Jonk et al., 2005; Jiang et al., 2016; Kempton et al., 2017; Parnell et al., 2001; Schubert et al., 2007; Song et al., 2018; Yang et al., 2018). The Niutitang Formation of the Lower Cambrian ($\epsilon_1 n$) is the main shale gas reservoir in the Micangshan tectonic zone (Tian et al., 2019a,b). Previous reports of hydrocarbon migration and accumulation histories in shale reservoir by using fluid inclusions are not a frequent as those for sandstone petroleum reservoirs, given that the grain sizes of the diagenetic minerals in mudstone are too small to trap fluids and form inclusions during diagenesis (Gao et al., 2015; Shang et al., 2016). However, shale reservoirs are often interbedded with mudstone, siltstone, fine sandstone and sandstone layers. A type of fracture-fill is commonly found in many mudstones in the form of fibrous veins, such as those composed of calcite, dolomite, quartz or sulphate, where abundant fluid inclusions are found (Gao et al., 2015; Liu et al., 2009a; Ni et al., 2016; Parnell et al., 2000). Therefore, shale samples with inclusions interbedded in calcite and quartz veins and interbedded sandstone samples have become the preferred objects for determining the hydrocarbon migration and accumulation histories in shale gas reservoirs (Gao et al., 2015; Liu et al., 2013; Xi et al., 2016).

In this paper, we tested the geochemical compositions and the homogenization temperatures of the entrapped fluid inclusions using microthermometry and microlaser Raman analysis. We combined the dataset of the fluid inclusions with bitumen vitrinite reflectance and tectonothermal history models to constrain the multi-staged accumulations in the Lower Cambrian to Neopoterozoic petroleum system in the Micangshan tectonic zone. This work will help to elucidate the hydrocarbon migration and accumulation histories and guide future shale gas and natural gas exploration and development.

2. Geological setting and field observations

The Micangshan tectonic zone lies on the northwestern margin of the Yangtze Plate and is a transitional orogenic belt between the Sichuan Basin and the Qinling Orogenic Belt, which is located to the east of the Longmenshan thrust belt but west of the Dabashan fold-thrust belt. This zone is an intraplate within the Yangtze Plate and is south of the Mianlue Suture Zone (Xu et al., 2009) (Fig. 1a, b). The formations of both limbs are composed of Sinian-Triassic sediments, with the Carboniferous-Devonian formations being absent. Overall, the study area was a passive continental margin, and a series of black shales were deposited in the Early Cambrian (Chang et al., 2010; Li et al., 2008; Tian et al., 2019a,b). The black shale and its overlying strata experienced deformation during subsequent tectonic movements. The lithology of outcrops in the region is variable after uplift and denudation. Numerous granitoids are distributed in the Micangshan massif and the Hannan massif, which formed during the Archaeozoic to Early Proterozoic period (Chang et al., 2010; Tian et al., 2010; Xu et al., 2009). Abundant Lower Paleozoic marine shales are mainly exposed on the western limbs of Micangshan. Permian to Cretaceous strata and SN-trending sub-folds are well-exposed in the eastern part (Fig. 1a). From north to south in the Micangshan tectonic zone, a distinct succession of Neogene-Quaternary sedimentary deposits (Hanzhong Basin), crystalline basement (Hannan and Micangshan massifs), Sinian-Triassic sedimentary deposits (Huijunba syncline) and Sinian-Cretaceous sedimentary cover (Norther Sichuan Basin) can be identified (Fig. 1c). Faults that developed between the basement and sedimentary cover are on a large scale and are oriented northeast-southwest (NE-SW), and most are thrust and slip faults (Fig. 1a). At the southern limb, a series of nearly latitudinally trending sub-folds developed in the sedimentary cover. The Lower Cambrian Niutitang Formation outcrops exhibit striped and irregular shapes, and the thickness revealed by three shale gas wells ranges from 85 m to 285 m. Moreover, the thickness of the Niutitang shales in some measured outcrop sections is greater than 200 m.

The drilling data from the SND-1 well revealed a 595-m thick marine sedimentary sequence from the Lower Cambrian, composed of the Niutitang ($\epsilon_1 n$), Shipai ($\epsilon_1 s$), Xiannvdong ($\epsilon_1 x$) and Canglangpu ($\epsilon_1 c$) Formations from bottom to top (Fig. 1c). The overlying Xiwangmiao Formation ($\epsilon_2 x$) of the Middle Cambrian and the underlying Dengying Formation ($Z_2 d$) of the Neopoterozoic are in unconformable contact with the Lower Cambrian. The Niutitang Formation consists mainly of lime mudstone and black/dark-grey organic-rich shale, which are considered to be the major source rocks. The Shipai Formation is composed of lime mudstone with thin siltstone interlayers. The Xiannvdong and Canglangpu Formations are mainly composed of limestone and mudstone with thin siltstone interlayers.

3. Samples and methods

3.1. Samples

The Niutitang Formation of the Lower Cambrian contains the most important hydrocarbon source rocks and shale gas reservoir in Micangshan tectonic zone. In this study, fluid inclusion samples were collected from eight outcrops in the Micangshan tectonic zone. Two samples were selected from the Niutitang Formation and the other six samples were selected from different formations that overlie and underlie the Niutitang Formation, respectively. The lithology of the samples are sandstone and shale with veins and carbonatite (Fig. 2). Sample F-B-3 is sandstone from the Canglangpu Formation. Sample F-B-4 is limestone with veins in the Xiannvdong Formation. Samples N-14 and Z-14 are silty shale and shale within calcite veins from the Niutitang Formation. Samples Y-10, C-09, F-B-2 and F-B-6 are dolomites from the Dengying Formation.

3.2. Methods

The experiments on fluid inclusions, including microscopic petrographic observations, microthermometric measurements and micro-laser Raman analyses, were conducted in the fluid-inclusion laboratory at the Xi'an Center of Geological Survey, China Geological Survey (CGS). Thermal re-equilibration caused by overheating and other post-entrapment processes always results in stretching, leakage and volume change of fluid inclusions (Barona et al., 2008; Bakker and Jansen, 1990; Dolson, 2016). Therefore, the smaller inclusions in well crystal form were selected to measure homogenization temperatures (T_h) values that approach the temperatures of original entrapment in this study. In view of the complex controls on fluorescence in hydrocarbon inclusions (George et al., 1997, 2007), laser Raman analysis was conducted instead of fluorescence colour studies under UV light to identify the components of the inclusions.

The fluid inclusions were carefully observed to identify their compositional types, gas–liquid ratios and spatial clustering using a Leica DMR-XP microscope with 50×–500× magnification. The petrography of fluid inclusion assemblages was first examined at

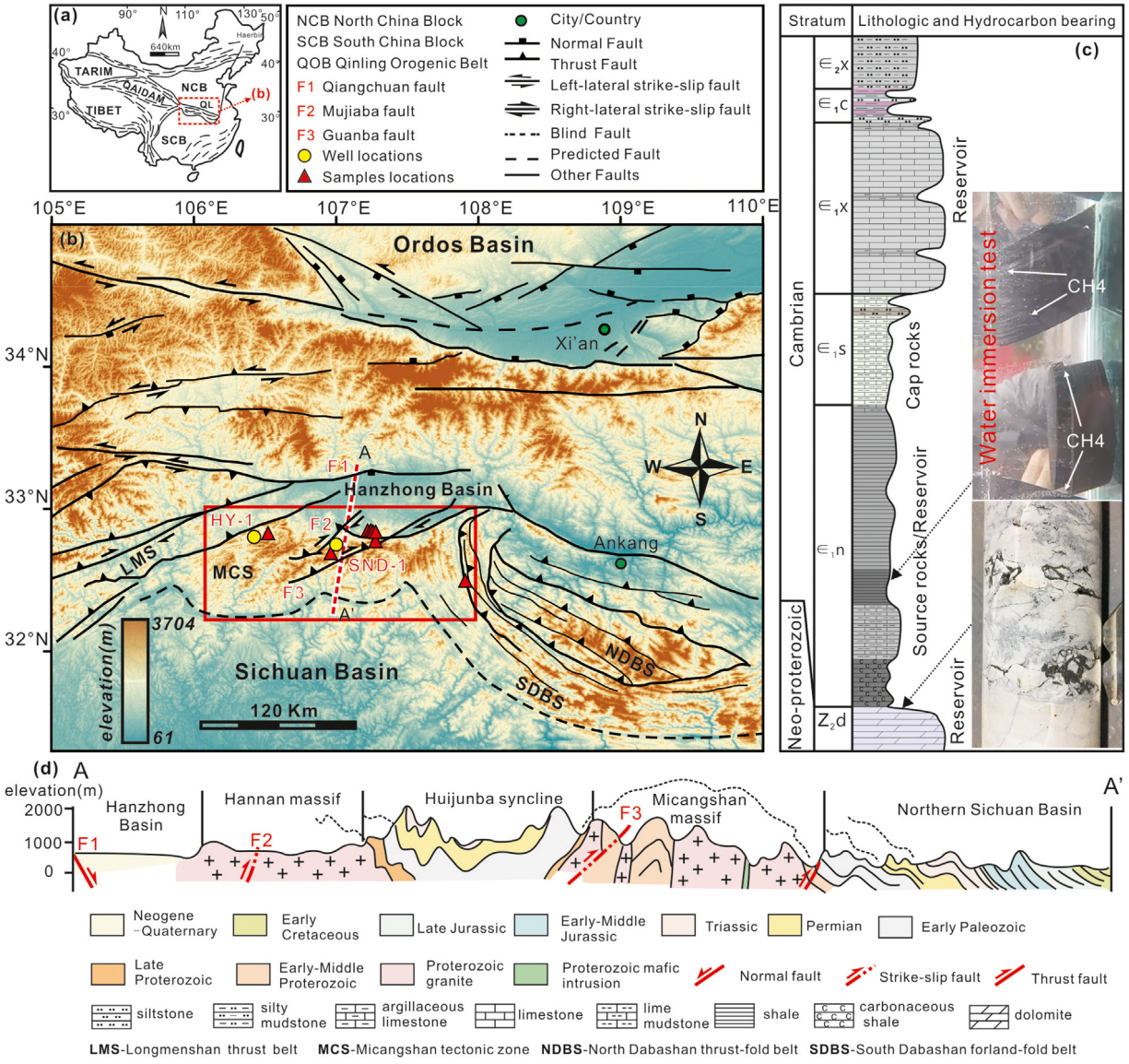

Fig. 1. (a∼b) Regional setting of the Micangshan tectonic zone and sampling points; (c) The lithological character histogram of the SND-1 Well in Micangshan tectonic zone; (d) Geological cross (A-A′)-section modified from Yang et al. (2013b).

low and then high magnifications. The selected samples were prepared as 100-mm-thick double-polished wafers using standard techniques for microthermometric measurements (Barona et al., 2008; Shepherd et al., 1985). Measurements were then performed using a Linkam TMS94 heating-freezing stage following standard procedures under a Zeiss-Axioskop40 petrographic microscope with a charge coupled device (CCD) camera. The of measurement precision is estimated to be ±1 °C for values between 25 °C and 200 °C. Homogenization temperatures of both hydrocarbon-bearing fluid inclusions and coeval aqueous fluid inclusions were measured; the freezing points of the aqueous fluid inclusions (T_m-ice) were measured. The heating rate was 10 °C/min during the initial stages of each heating run and was reduced to 1–2 °C/min close to the phase change points. Salinity was determined by freezing the inclusion with liquid nitrogen and then heating the frozen inclusion until the last solid phase melted; the values were calculated using the ice points of H_2O–NaCl (Bodnar, 1993). Micro-laser Raman analyses were performed using a Renishaw inVia Microprobe to identify the components of the fluid inclusions. The semiconductor laser source is green light Ar-ion with $\lambda = 514.5$ nm, an exciting time of 2 s per spectrum with a 30-mW laser power, a 20-μm spectrograph slit and 2-cm^{-1} resolution ratio. Based on the observations of the microlithofacies of the inclusions, gas–liquid inclusions with complete shapes were selected for the laser Raman experiments on the gas and liquid phases. The relative molar fractions (mol %) of the components in a gas mixture was obtained using the following Eq. (1):

$$X_a = \frac{\frac{A_a}{\sigma_a \zeta_a}}{\sum \frac{A_i}{\sigma_i \zeta_i}} \tag{1}$$

where X_a, A_a, σ_a and ζ_a, are the molar fraction, the band area, the Raman cross-section and the instrumental efficiency for gas a, respectively, while ΣA_i, σ_i, and ζ_i represents the sum of values for all gas species in the fluid inclusion (Beeskow et al., 2005; Burke, 2001; Frezzotti et al., 2012; Morizet et al., 2009; Schrötter and Klöckner, 1979).

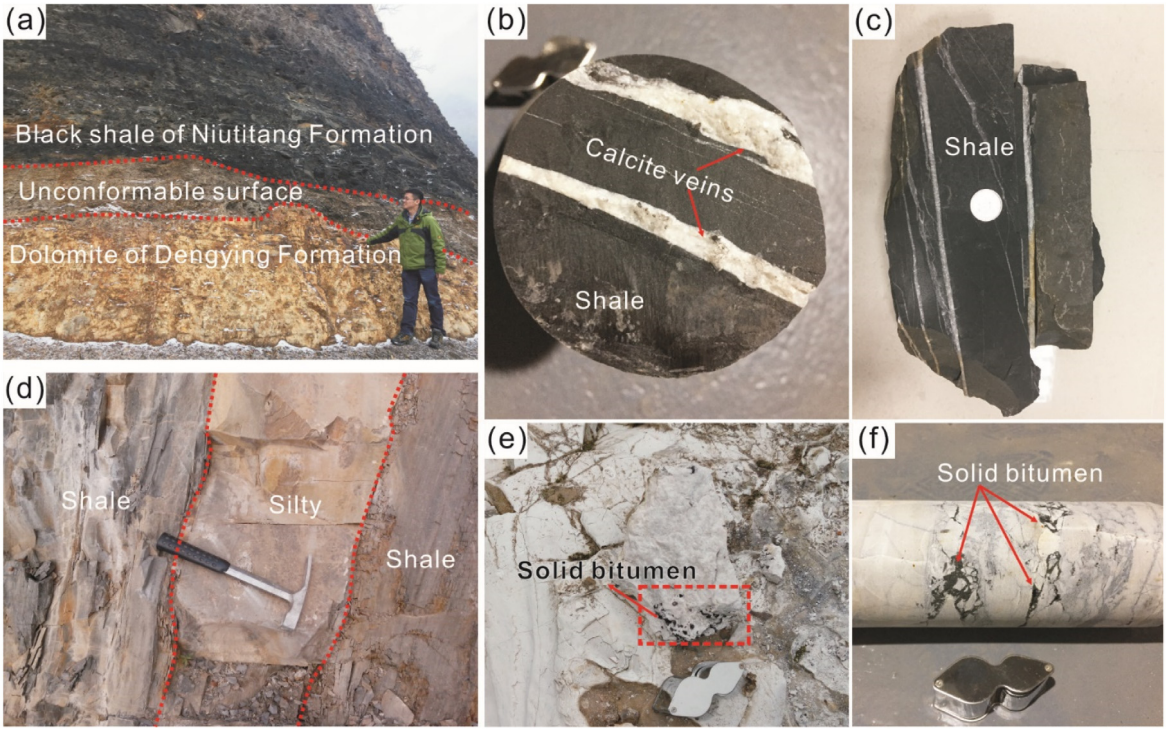

Fig. 2. Pictures of samples (a) The Niutitang Formation of the Lower Cambrian is in unconformable contact with the underlying Dengying Formation of the Neoproterozoic; (b∼c) Black shale samples from the Niutitang Formation with calcite veins; (d) Dark grey silty shale with thin siltstone interlayers from the Niutitang Formation; (e∼f) Corrosion holes and micro-fractures developed in off-white dolomite samples from the Dengying Formation and filled with black bitumen.

4. Results

4.1. Microlithofacies of fluid inclusions

Microlithofacies of fluid inclusions is the important evidence for confirming the phases and textural relationships between the fluid inclusions and host minerals. Three fluid inclusion types were identified based on the phases by microscopic observations at room temperature (25 °C), and they were gas–liquid inclusions, gas inclusions and solid bitumen inclusions. The gas–liquid phase inclusions were abundant and were recorded in all samples, with the gas–liquid ratios ranging from 20% to 80% with clear boundaries. The gas–liquid inclusions were translucent and mainly distributed in the large calcite and quartz particles with oval, quadrate and irregular shapes of different sizes ranging from 1.8 μm to 8.1 μm. High-density methane inclusions in shale reservoirs have been found in the Sichuan Basin with a light grey to dark grey colour in transmitted light (Gao et al., 2015; Liu et al., 2009a,b). Only one gas phase (or close to) inclusion with similar optical characteristics was found in Sample F-B-3 from the Canglangpu Formation ($\epsilon_1 c$), and none was found in the other samples. The opaque semi-solid or solid phase inclusions occurring within individual fluid-inclusion assemblages in dark grey or black colours probably were bituminous inclusions with coatings of solid bitumen after oil cracking (Fig. 3).

4.2. Raman spectroscopy

Raman spectroscopy is a versatile non-destructive technique for fluid inclusion analysis, with a wide range of applications ranging from qualitative detection of solid, liquid and gaseous components (Frezzotti et al., 2012). The characteristic Raman bands for most important geological fluids are reported in previous research for qualitative identification of major fluid inclusion components (Azbej et al., 2007; Brunsgaard et al., 2002; Davis and Oliver, 1972; Dubessy et al., 2001; Guillaume et al., 2003; Zhang et al., 2007). The Raman spectroscopy results of the host minerals show that the Raman peaks for quartz and calcite are evident in all samples (Fig. 4). The Raman spectroscopy results for the gas phases show that Raman peaks for CH_4, N_2 and CO_2 were identified. The Raman peaks for CH_4 were clear in most samples and were not apparent in some samples due to background fluorescence. The Raman spectra of CH_4 in samples from the Niutitang and the Dengying Formations range from 2915.87 to 2916.49 cm^{-1}, which approximate the typical Raman spectrum of CH_4 (2917 cm^{-1}). However, the Raman spectra of CH4 in samples from the overlying Xiannvdong ($\epsilon_1 x$) and Canglangpu ($\epsilon_1 c$) Formations ranges from 2908.25 to 2909.1 cm^{-1} (Fig. 4), which has similar spectral characteristics of high-density methane inclusions and indicated high internal pressures in those inclusions (Lu et al., 2007; Liu et al., 2013). The main gaseous components of the fluid inclusions in the Niutitang Formation were CH_4 and CO_2, and molar proportions of CH_4 ranged from 19.4% to 81.2% with an average of 47.1%. Different from the Niutitang Formation, the main gaseous components of fluid inclusions in Canglangpu ($\epsilon_1 c$), Xiannvdong ($\epsilon_1 x$) and the Dengying Formations ($Z_2 d$) were CH_4 and N_2, the molar proportions of CH_4 were over a broad range, extending from 27.1% to 92.8% with an average of 67.5%. N_2 in inclusions from the Dengying Formation were more frequent than those in the Canglangpu and Xiannvdong Formations with a range of 26.6%–72.9%. Moreover, some H_2 at 0.8% proportion was observed in Sample F-B-3 (Fig. 5). The main components of the liquid phase were almost entirely H_2O and small amounts of CH_4 with a range of 0.03%–0.13% that was dissolved in water. Therefore, all gas–liquid inclusions could be divided into CH_4–N_2–H_2O and CH_4–CO_2–H_2O systems based on the main components.

4.3. Fluid inclusion microthermometry

The homogenization temperatures (T_h) of eight gas–liquid inclusions were measured, and the microthermometric data for

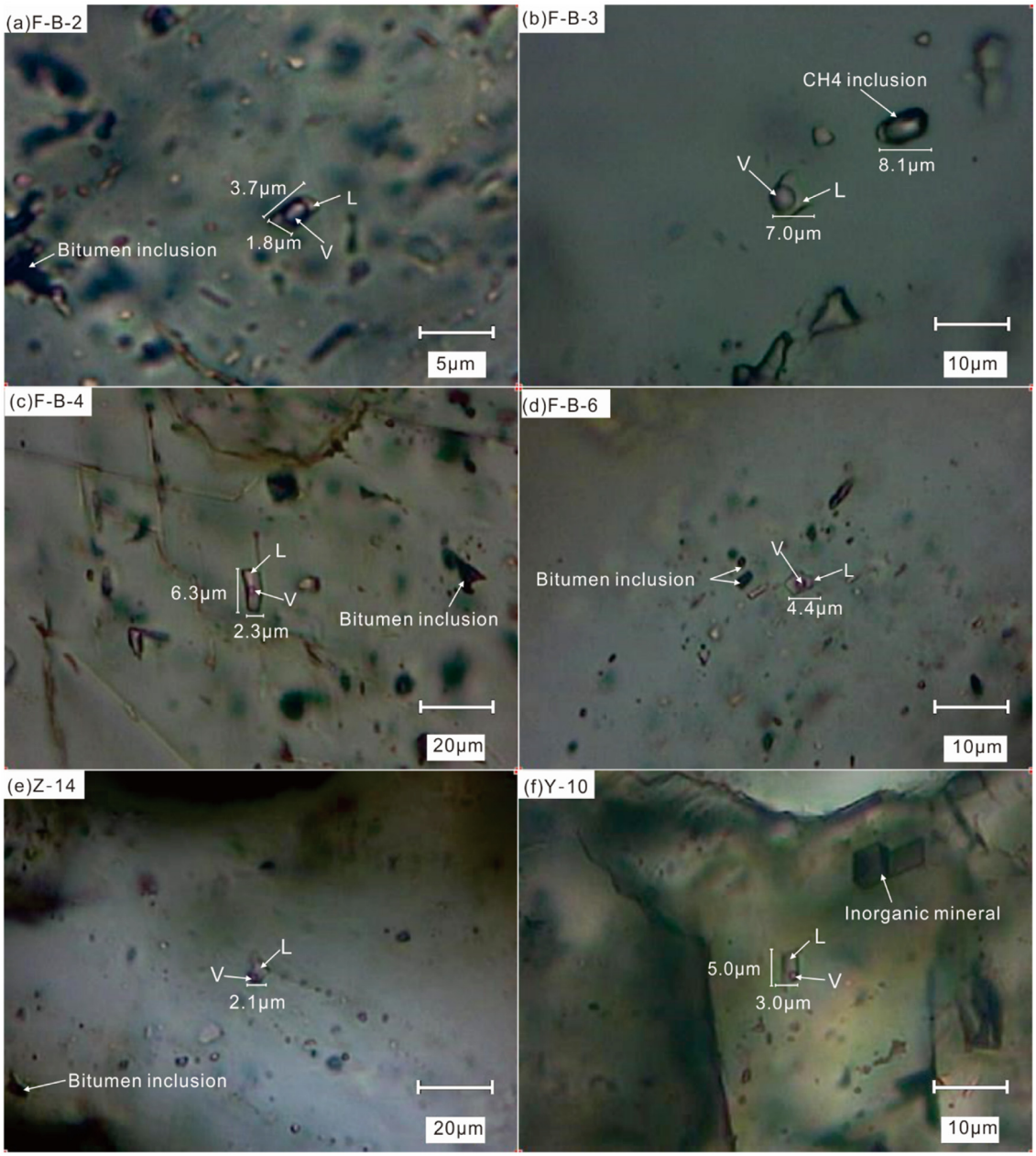

Fig. 3. Photomicrographs of typical fluid inclusions in transmitted light. (a) An oval gas–liquid inclusion measuring 3.7 μm long and 1.8 μm wide and some black irregular bitumen inclusions was entrapped in a calcite grain in a dolomite sample from the Dengying Formation (Z_2d); (b) A dark grey gas inclusion with 8.1-μm length and a gas–liquid inclusion with 7.0-μm length and 60% gas–liquid ratio were entrapped in quartz in a siltstone sample from the Canglangpu Formation (ϵ_1c); (c) A quadrate gas–liquid inclusion with 6.3-μm length and a 20% gas–liquid ratio and black irregular bitumen inclusions was entrapped in a calcite vein in a limestone sample from the Xiannvdong Formation (ϵ_1x); (d) An oval gas–liquid inclusion with 4.4-μm length and a 20% gas–liquid ratio and dark grey bitumen inclusions was entrapped in quartz in a dolomite sample from the Dengying Formation (Z_2d); (e) Several small and near round gas–liquid inclusions were entrapped in quartz particles as linear forms in a siltstone sample from the Niutitang Formation (ϵ_1n); (f) A rhombic gas–liquid inclusion with a 4.5-μm length and a 20% gas–liquid ratio and an inorganic mineral inclusion were entrapped in calcite particles in a dolomite sample from the Dengying Formation (Z_2d).

fluid inclusions are summarized in Fig. 6 and Table 1. The results show that the homogeneous temperatures of (T_h) fluid inclusions in the Niutitang Formation (ϵ_1n) ranged from 157 to 197 °C and the corresponding ice-melting temperatures (T_m-ice) ranged from −5.1 to −3.0 °C (from 4.9 to 8.0 wt% NaCl.eqv). The Th of fluid inclusions in the Dengying Formation (Z_2d) showed two intervals that ranged from 226 °C to 235 °C and from 295 °C to 336 °C and yielded T_m-ice from −21.6 to −12.7% °C (from 16.7 to 24 wt% NaCl.eqv). We observed the highest T_h ranges, that is, from 368 °C to 399 °C, in the Canglangpu Formation (ϵ_1c) and from 364 °C to 465 °C in the Xiannvdong Formation (ϵ_1x), but their salinity and ice-melting temperatures differed in that the T_m-ice ranged from −12.8 to −11.6% °C (from 15.6 to 16.8 wt% NaCl.eqv) in the Canglangpu Formation (ϵ_1c) and ranged from −1.7 to −1.3% °C (from 2.2 to 2.9 wt% NaCl.eqv) in the Xiannvdong Formation (ϵ_1x).

The results of microthermometry show that the T_h, salinity and T_m-ice of the fluid inclusions in different formations exhibit significant differences. The T_h values for fluid inclusions are higher in the Xiannvdong and Canglangpu Formations and are lowest in the Niutitang Formation. The T_m-ice of the Dengying Formation was lowest but had the highest salinity. Oppositely, the T_m-ice in the Xiannvdong Formation was highest but with the lowest salinity. The distributions of T_h and salinity and their relationships may indicate that fluid inclusions were entrapped

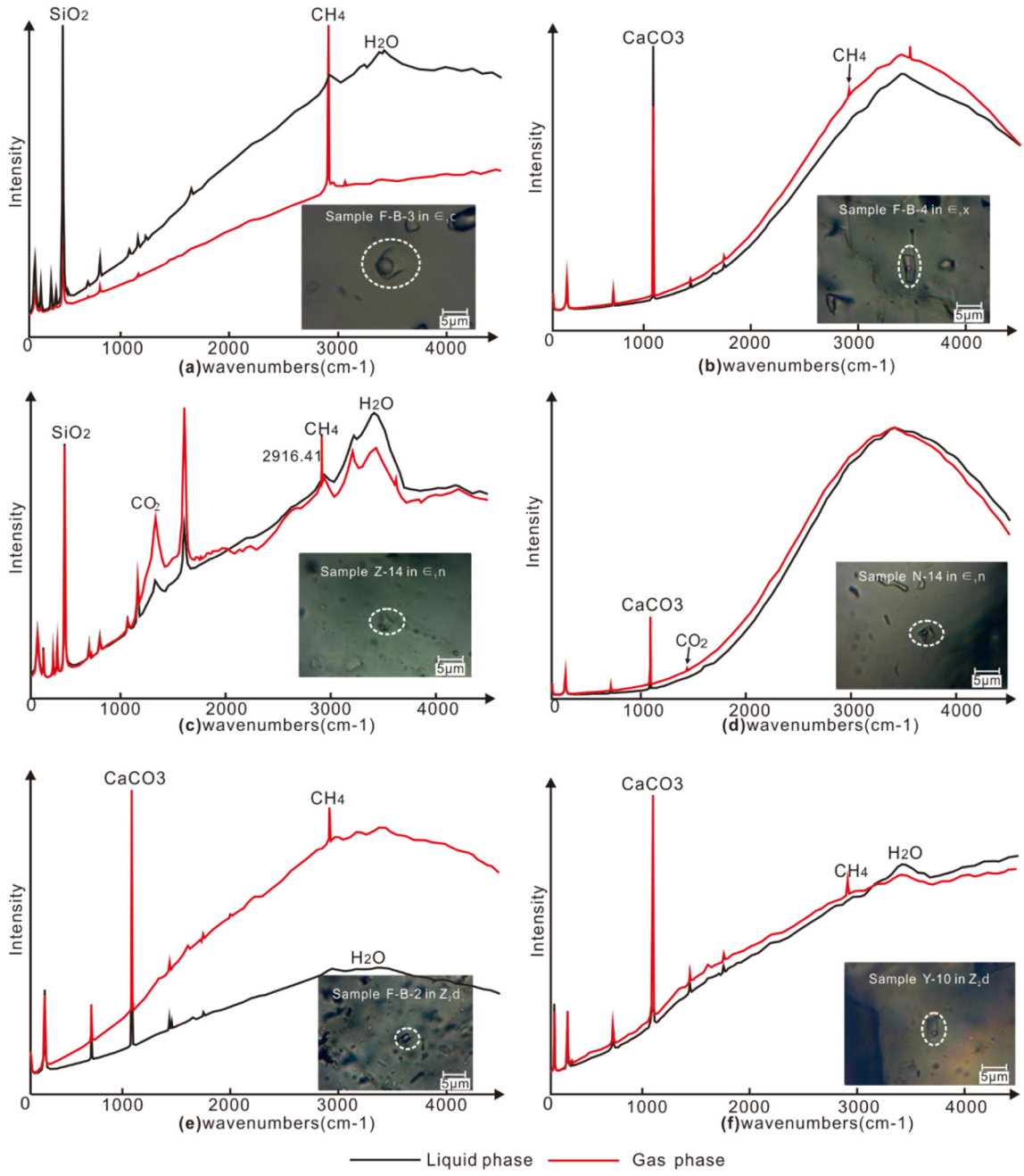

Fig. 4. Typical Raman spectral images of gas–liquid inclusions in the Lower Cambrian to Neopoterozoic.

in a separate, closed fluid environment, which can be interpreted as multi-staged hydrocarbon filling and accumulation in the Micangshan tectonic zone.

5. Discussion

5.1. Fluid inclusion entrapment

Homogenization temperatures and salinities imply the source information of aqueous fluids in reservoirs, which can be used to define trapping conditions and fluid migration routes (Dolson, 2016). In this study, the relationship between homogenization temperatures and salinities is nonlinear; the salinity first increased and then decreased with increasing T_h and a T_h value of approximately 250 °C is the change point (Fig. 6c), which is consistent with previous research (Wang et al., 2000; Yang et al., 2013a; Zhang et al., 2014).

The T_h recorded from many fluid inclusions hosted in quartz and calcite are greater than expected for a typical sedimentary basin (Walderhaug, 1994), indicating that the temperatures during diagenesis were higher than the expected temperatures during the maximum burial history (Barona et al., 2008). Fluid inclusions were usually produced in areas where active mineralization occurred, such as systems of geothermal fields and hydrothermal ore deposits (Okubo, 2005). Therefore, an alternative mechanism of heating by high temperature fluids circulating in the sequence was used to explain the abnormal high T_h values (Barona et al., 2008; Wycherley et al., 2003).

The equivalent vitrinite reflectances (VR_{equ}%) from bitumen vitrinite reflectances (R_b%) (Table 2) and basin modelling data (Fig. 9) indicate that the higher T_h values recorded in the fluid

Table 1
Microthermometric data of the fluid inclusions.

Sample number	Location	Formation	Host mineral	T_h/°C	T_m-ice/°C	Salinity /wt% NaCl. eqv
N-14	106°27′34.2″E 32°57′45.0″N	$\epsilon_1 n$	calcite	168 166 157	−5.1 −4.8 −4.8	8.0 7.6 7.6
Z-14	N32°29′24″ E107°56′52.1″	$\epsilon_1 n$	quartz	197 195 190 189 189	−3.6 −3.4 −3.4 −3.1 −3.0	5.8 5.5 5.5 5.1 4.9
Y-10	106°59′50″E 32°42′40.0″N	$Z_2 d$	calcite	226 235 228 226	−20.4 −21.6 −20.1 −18.8	23.0 24.0 22.5 21.8
C-9	107°16′13.0″E 32°44′36.2″N	$Z_2 d$	quartz	336 333 332	−14.5 −14.1 −14.0	18.3 18.0 17.9
F-B-2	107°14′56″E 32°49′8.4″N	$Z_2 d$	calcite	318 315 315	−15.7 −14.8 −14.6	19.4 18.6 18.3
F-B-3	107°15′05″E 32°48′48″N	$\epsilon_1 c$	quartz	399 399 391 391 371 368	−12.6 −12.8 −12.2 −11.8 −11.6 −11.6	16.6 16.8 16.2 15.8 15.6 15.6
F-B-4	107°15′23″E 32°48′56″N	$\epsilon_1 x$	calcite	465 368 364	−1.7 −1.4 −1.3	2.9 2.4 2.2
F-B-6	107°14′52″E 32°49′8.4″N	$Z_2 d$	quartz	305 300 295	−14.5 −14.0 −12.7	18.3 17.9 16.7

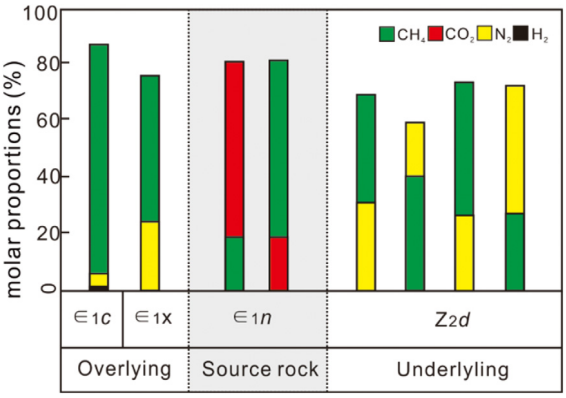

Fig. 5. Gaseous components of the fluid inclusions.

inclusions of the Canglangpu ($\epsilon_1 c$), Xiannvdong ($\epsilon_1 x$) and the Dengying ($Z_2 d$) Formations were not related to the burial history. Moreover, the T_h values of the overlying Canglangpu and Xiannvdong Formations were considerably higher than those underlying the Niutitang to the Dengying Formations. These data may provide evidence for hot-fluid migration events in association with magmatism during depositional stages of $\epsilon_1 c$, $\epsilon_1 x$ and $Z_2 d$ when the inclusions were entrapped.

The kerogen type of the organic-rich matter in the Niutitang shale in the Micangshan tectonic zone is dominated by Type I (Fu et al., 2018; Tian et al., 2019a,b), which indicates good potential for oil generation, but no oil inclusions were found in this study. The absence of oil inclusions can be interpreted as follows: (1) Mudshale was the main lithology of the Niutitang Formation, and the fine diagenetic particles were thought to be disadvantageous during diagenesis and for inclusion entrapment for which oil inclusions failed to be entrapped. (2) The oil inclusions were entrapped in the stage of oil generation, and the oil in the inclusions had been cracked into CH_4, H_2O, bitumen and other components (Okubo, 2005); the colour of the oil inclusions turned fuscous (Liu et al., 2009b; Suchý et al., 2010; Zhang et al., 2009) in the post-entrapment process. The occurrences of black solid bitumens in some inclusions are typical products of degradation of reservoir oils (Rogers et al., 1974). In the Micangshan tectonic zone, abundant black residual solid bitumen can be seen in the dissolution pores and micro-fractures in dolostone in the Dengying Formation (Fig. 3) and bitumen inclusions were also found in the $\epsilon_1 n$ and in other formations (Fig. 3). Therefore, our preferred hypothesis explaining the lack of oil inclusions in the Niutitang Formation in the Micangshan tectonic zone is that the oil in the inclusions was cracked.

The frequency of CH_4 Raman spectroscopy may change as a function of the composition and density in a fluid inclusion. Utility of the shift of the peak positions for gas species can be as a sensitive monitor for pressure and density, and peak position of CH_4 shift to lower relative wavenumbers as density or pressure increases (Fabre and Oksengorn, 1992; Hansen et al., 2001a,b, 2002; Seitz et al., 1993, 1996). Some systematic research has been conducted to determinate the internal pressures of fluid inclusions by analysing the Raman characteristics of CO_2, N_2, CH_4 and their mixtures changing with pressure, and the methods of pressure determination by Raman spectral parameters in CH_4-CO_2 and CH_4-N_2 systems were proposed (Chen et al., 2005; Lu et al., 2007; Roedder and Bodnar, 1980; Seitz et al., 1993, 1996). In this study, the Raman results show that the gaseous components of the two-phase aqueous inclusions were CH_4-CO_2 in the Niutitang Formation and that was CH_4-N_2 in the other formations. Five samples have clear CH_4 Raman peaks, and their internal pressure of the two-phase aqueous inclusions in the Niutitang and Dengying Formations were less than 5 MPa and considerably larger than 70 MPa in the Xiannvdong and Canglangpu Formations (Fig. 7).

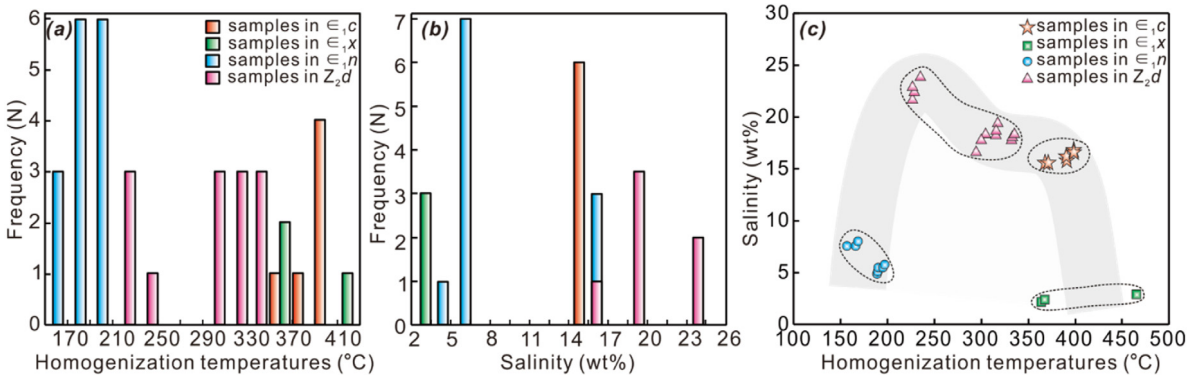

Fig. 6. Histograms showing the distribution of the homogenization temperature (a) and salinity (b) of fluid inclusions and cross-plot of them (c).

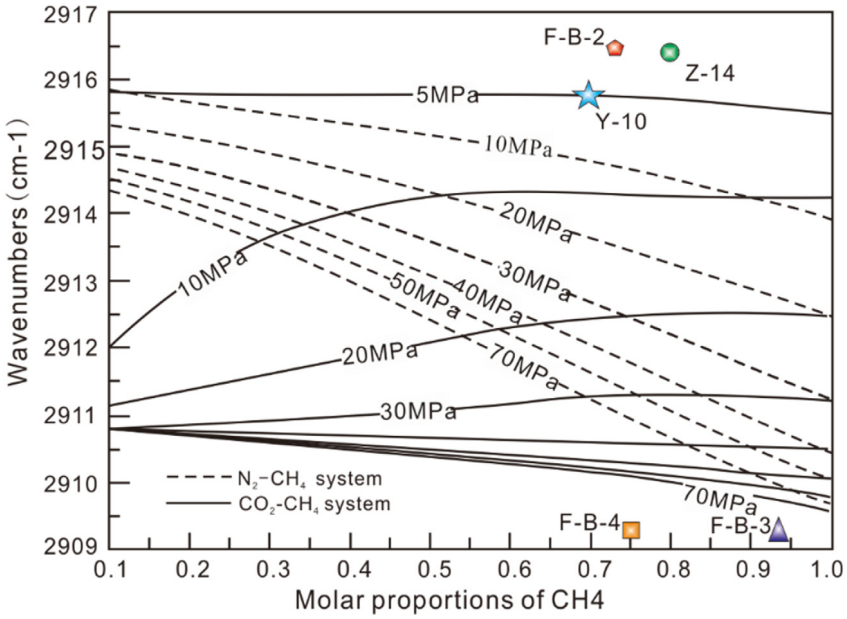

Fig. 7. Determination of internal pressure of fluid inclusion of CH_4–N_2 and CH_4–CO_2 systems.
Source: Base map modified from Seitz et al. (1993, 1996).

Therefore, the model of the fluid inclusion entrapment process can be explained by the data from Raman spectroscopy, T_h and salinity in different formations.

5.1.1. Fluid inclusions entrapped in the Dengying Formation

The organic-rich shale of the Niutitang Formation began to generate oil when the temperature rose to the "oil threshold". Part of the oil migrated into the underlying Dengying Formation along the micro-fractures and was stored in the dissolved pores. The oil in the pores was then cracked with the increase in temperature and black solid bitumen was a residual component in those dissolved pores (Fig. 2e, f). Upwardly migrating invasive fluids with inhomogeneous, circulating high temperatures occurred in the Dengying Formation during oil cracking and the gas from pyrolysis was entrapped as fluid inclusions. The temperatures at the bottom of the upward invasive fluids was greater (295 °C–399 °C) with salinities ranging from 16.7% to 19.4% (I) and temperatures near the paleosurface were lower (226 °C–235 °C) with salinity ranging from 21.8% to 24.0% (II). The N_2 in the inclusions of the Dengying Formation may have been derived from rainwater infiltration along the unconformable contact between the Dengying and the Niutitang Formations (Fig. 8).

5.1.2. Fluid inclusions entrapped in the Niutitang Formation

Only a few oil inclusions were formed in the "oil threshold" because of the fine diagenetic particles in the Niutitang Formation. Subsequently, the oil inclusions cracked into gaseous hydrocarbons and were destroyed with the increasing temperatures and pressures, the hydrocarbon migrated out and solid bitumen remained as bitumen inclusions, especially in calcite particles (Fig. 3). With the thermal evolution, abundant CH_4 and some CO_2 were formed at "dry gas stage" in the Niutitang Formation, when the organic-rich shale was in a highly overmature state, and the gaseous components were entrapped during the diagenetic process and were ultimately preserved in quartz and calcite veins distributed in the shale lamellations. The entrapment conditions were reflected by the salinity and T_h values of fluid inclusions at temperatures of 157 °C∼197 °C and with salinities ranging from 4.9% to 8.0% (Fig. 8).

5.1.3. Fluid inclusions entrapped in the Xiannvdong and Canglangpu Formation

The Raman spectra of CH_4 in samples from the overlying Xiannvdong (ϵ1x) and Canglangpu (ϵ1c) Formations ranges from 2908.25 to 2909.1 cm^{-1}, which has characteristics similar to spectra of high-density methane inclusions. The appearance of high-density methane inclusions often reflects a special geological and

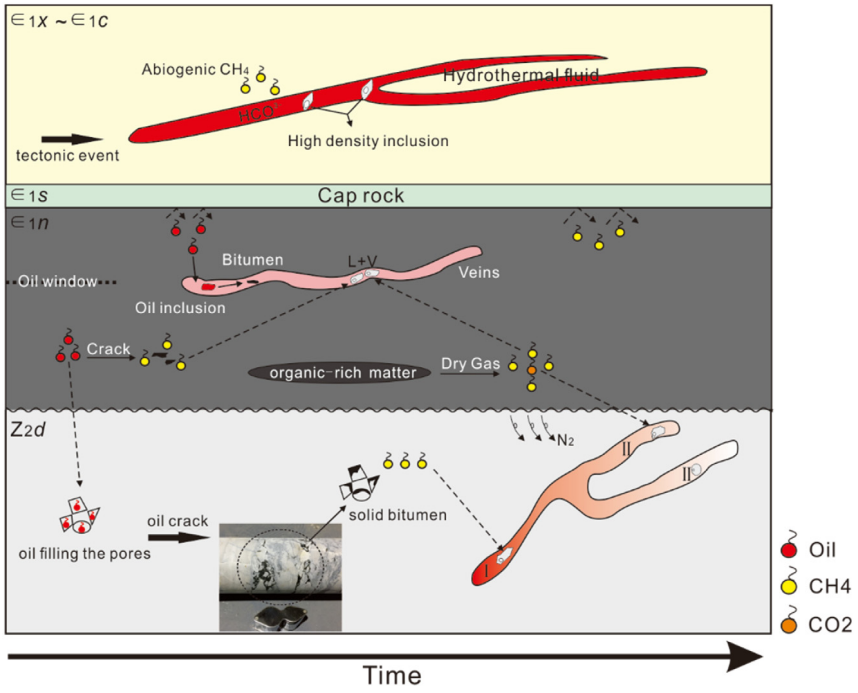

Fig. 8. Mode of hydrothermal fluid activity and fluid inclusion.

geochemical environment. The high-density methane inclusions could have been caused by cracking of oil inclusions, serpentinization and hydrothermal fluids (Chen et al., 2007; Horita and Berndt, 1999; Hurai et al., 2006; Liu et al., 2013). The oil inclusions entrapped in the quartz and calcite particles were buried in the early stage and then started to crack into gaseous hydrocarbons and solid bitumen with the increasing temperatures of over 180 °C, while the products of oil cracking were retained in the unbroken inclusions that lead to a high internal pressures in the inclusions. Based on the process of oil cracking, the Raman peak for bitumen should be visible in Raman spectroscopy. In this study, the Raman peaks for bitumen in the inclusions were invisible, meaning that high internal pressures may be not have been caused by cracking of oil inclusion. Moreover, the overlying Shipai Formation provided a good cap rock, composed of mudrock and silt, and it appears that oil from the Niutitang Formation did not easy migrate upward to Xiannvdong and Canglangpu Formations. Hurai et al. (2006) suggest high density methane inclusion as important information to reflect a tectono-thermal event. Abiogenic CH_4 could have been formed from dissolved bicarbonate (HCO^{3-}) under hydrothermal conditions and serpentinization at temperatures below 400 °C (Chen et al., 2007; Horita and Berndt, 1999). The Micangshan tectonic zone is located on the coupling part between the Sichuan Basin and the Qinling orogenic belt. The transitory high temperature fluid events may have been caused by regional tectonomagmatism since the Early Cambrian (Chang et al., 2010). The abiogenic CH_4 may have formed in hydrothermal fluids at temperatures ranging from 364 °C to 399 °C and with salinities ranging from 2.2% to 2.9% in the Xiannvdong Formation and salinities of 15.6% to 16.8% in the Canglangpu Formation, with CH_4 migration being synchronous with these high-temperature fluids (Fig. 8).

5.2. Hydrocarbon migration, filling and accumulation

The ages of hydrocarbon migration, filling and accumulation can be evaluated by combining the Th data with the corresponding burial-thermal evolution model (Dolson, 2016; Yang et al., 2020). To better understand the relationships between the fluid inclusion data and thermal history and to clarify the hydrocarbon migration of the Lower Cambrian, we modelled the burial and thermal history of the SND-1 and HY-1 wells using Platte River BasinMod^{TM} software (Fig. 9a and c). The thermal history used to model the vitrinite reflectance data are shown in Fig. 9b and d and Table 2. The data used for burial history modelling, such as uplift periods and erosion thicknesses, were referenced in previous research (Chang et al., 2010; Shi and Shi, 2014; Tao et al., 2009; Tian et al., 2012; Wang and Xiao, 2010), and the stratigraphic modelling was based on the SND-1 Well and HY-1 wells. The high T_h of the fluid inclusions in the Canglangpu, Xiannvdong and the Dengying Formations conflicted with their burial temperatures. Therefore, the T_h data of inclusions in the Niutitang Formation were used and combined with burial-thermal histories.

The Micangshan tectonic zone developed in a passive continental margin in an extensional tectonic environment in the Early Cambrian (Chang et al., 2010; Li et al., 2008; Tian et al., 2019a,b). Water invaded the Micangshan area along the Longmenshan tectonic zone and began organic-rich marine deposition. The burial model shows that rapid subsidence started at 290 Ma and the organic matter in the Niutitang Formation was into the "oil threshold" at ~277 Ma. The oil then migrated to the Dengying Formation and was stored in dissolved pores and micro-fractures. The oil started to crack as gaseous hydrocarbons with the thermal evolution of main gas stage, the CH_4-bearing and bitumen inclusions were entrapped in the Niutitang and Dengying Formations. Abundant CH_4 was formed when the organic-rich matter attained the "dry gas stage" and was mainly stored in the micro-nano pores and fractures of the Niutitang shales due to their compactness and the good cap rock of Shipai Formation. There may have been two gas accumulation events in the Micangshan tectonic zone (Fig. 9): the inclusion samples collected from the Niutitang Formation were emplaced at 212–198 Ma with burial depths of 4898–5743 m and from 173–166 Ma with burial depths of 5988~6310 m, respectively. The gas sources in the first accumulation stage may have mainly been from oil cracking and those in the second accumulation stage may have been from dry

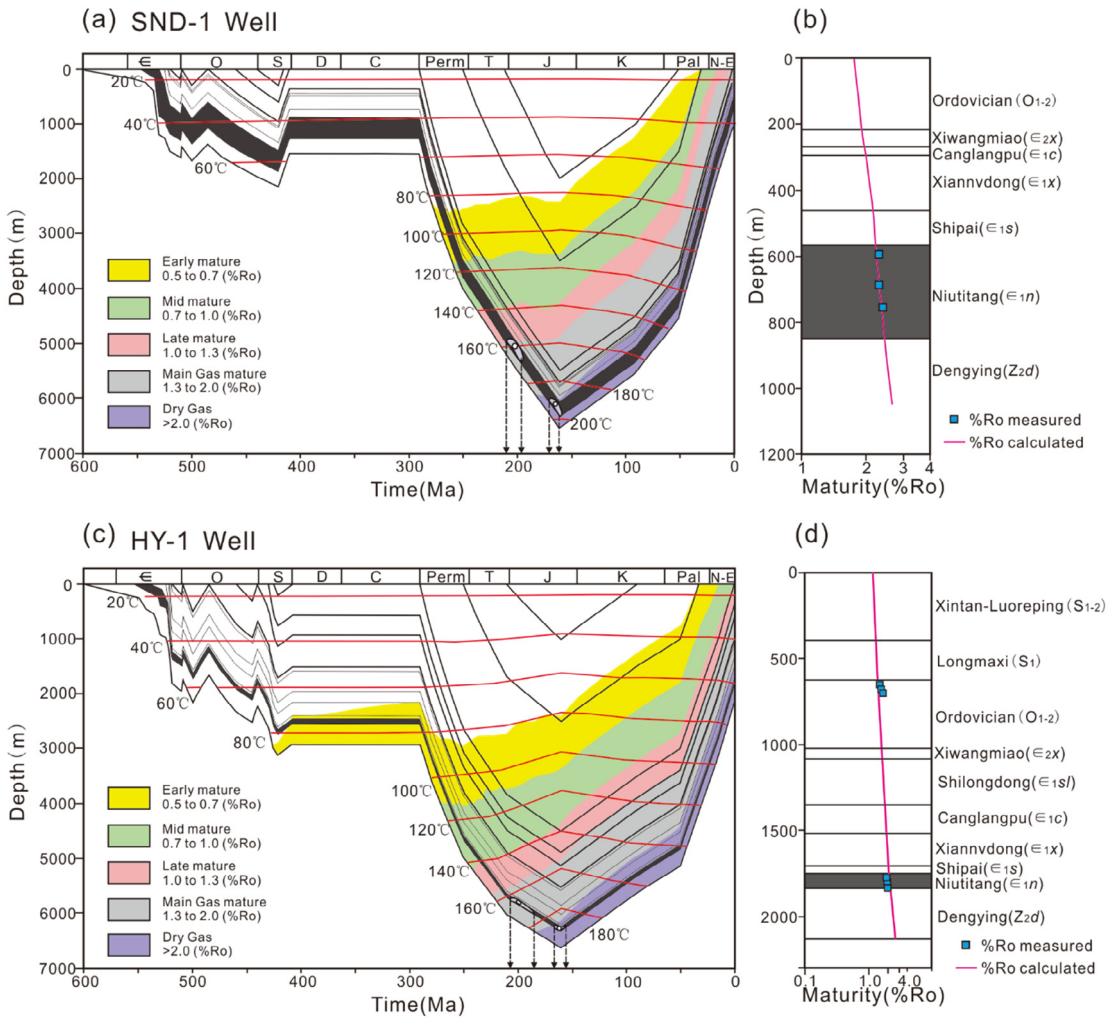

Fig. 9. Thermal histories and hydrocarbon filling stages.

gas. The rapid uplift and denudation of strata started under the influence of intra-continental orogeny in the Late Jurassic (Chang et al., 2010; Tian et al., 2019a,b; Yang et al., 2013b), and the transitory high-temperature fluid events occurred and invaded the Xiannvdong and Canglangpu Formations. Abiogenic CH_4 then formed in the hydrothermal fluids.

6. Conclusions

Abundant CH_4-bearing fluid inclusions were obtained in the Lower Cambrian to Neoproterozoic petroleum system and provided direct evidence for hydrocarbon migration in the Micangshan tectonic zone. The characteristics of the petrography, spectroscopy and microthermometry of fluid inclusions in the petroleum reservoirs are different from each other and show that the formation of natural gas was multifactorial in this petroleum system. The gas in the Niutitang ($\epsilon 1n$) and Dengying ($Z2d$) reservoirs was mainly from oil cracking and dry gas, and the gas in the Xiannvdong ($\epsilon 1x$) and Canglangpu ($\epsilon 1c$) reservoirs may be abiogenic and formed in hydrothermal fluids by regional tectonothermal events. Based on the fluid inclusion analyses and combined with the reservoir thermal models of the SND-1 Well and HY-1 Well, three stages of hydrocarbon charge were identified in the Lower Cambrian to Neopoterozoic petroleum system in the Micangshan tectonic zone. The stage of oil charge first began in the Early Permian (∼277 Ma); the stage of gas charge from oil cracking occurred in the Late Triassic to Early Jurassic (212–198 Ma); and the stage of gas charge from dry gas occurred in the Middle Jurassic (173–166 Ma). The gas of mixed origin from the Niutitang shale source occurred in the nanoscale pores as a self-reservoir, rather than as an effective gas source for the overlying reservoirs.

Declaration of competing interest

The authors declare that they have no known competing financial interests or personal relationships that could have appeared to influence the work reported in this paper.

CRediT authorship contribution statement

Tao Tian: Conceptualization, Methodology, Software, Resources, Data curation, Writing - original draft , Writing - review & editing, Project administration, Funding acquisition. **Peng Yang:** Conceptualization, Methodology, Validation, Formal analysis, Data curation, Writing - original draft, Writing - review & editing, Visualization, Funding acquisition. **Zhanli Ren:** Conceptualization, Methodology, Supervision, Writing - review & editing, Project administration, Funding acquisition. **Deliang Fu:** Formal analysis, Investigation, Project administration. **Shixin Zhou:** Supervision, Methodology, Writing - review & editing. **Fu Yang:** Investigation. **Jing Li:** Investigation.

Table 2
Bitumen reflectance and vitrinite equivalent reflectance data from SND-1 and HY-1 Wells.

Well	Depth (m)	Formation	R_b (%)	VR_{equ} (%)
SND-1	593.0	$\in_{1n}$	2.95	2.30
	685.0		2.97	2.30
	755.0		3.02	2.40
HY-1	674.3	$\bigcirc_{1x}$	1.77	1.52
	674.7		1.78	1.53
	677.0		1.81	1.55
	677.9		1.87	1.59
	679.7		1.84	1.57
	681.6		1.89	1.60
	682.2		1.81	1.55
	683.2		1.72	1.49
	684.6		1.81	1.55
	691.4		1.92	1.62
	693.1		1.94	1.64
	694.3		1.97	1.66
	696.4		1.93	1.63
	698.0		2.03	1.70
	699.2		2.17	1.79
	704.8		2.21	1.82
	1800.2	$\in_{1n}$	2.47	2.00
	1803.9		2.42	1.96
	1806.8		2.61	2.09
	1807.2		2.56	2.06
	1808.2		2.65	2.12

Note: R_b, bitumen reflectance (%); VR_{equ}, equivalent vitrinite reflectance calculated by $VR_{equ} = 0.3195 + 0.679R_b$ (Feng and Chen, 1988).

Acknowledgements

This study was supported by the Open Found of Shandong Key Laboratory of Depositional Mineralization and Sedimentary Minerals (Grant No. DMSM20190022), the Independent Project of Key Laboratory of Coal Exploration and Comprehensive Utilization, Ministry of Natural Resources (Grant No. ZP2019-2), the State Key Program of National Natural Science Foundation of China (Grant No. 41630312) and National Science and Technology Major Project (Grant Nos. 2016ZX05003002-004 and 2016B-05-02)

References

Azbej, T., Severs, M.J., Rusk, B.G., Bodnar, R.J., 2007. In situ quantitative analysis of individual H_2O–CO_2 fluid inclusions by laser Raman spectroscopy. Chem. Geol. 237, 255–263. http://dx.doi.org/10.1016/j.chemgeo.2006.06.025.

Bakker, R.J., Jansen, J.B.H., 1990. Preferential water leakage from fluid inclusions by means of mobile dislocations. Nature 345 (6270), 58–60. http://dx.doi.org/10.1038/345058a0.

Barona, M., Parnell, J., Mark, D., Carr, A., Przyjalgowski, M., Feely, M., 2008. Evolution of hydrocarbon migration style in a fractured reservoir deduced from fluid inclusion data, Clair Field, west of Shetland, UK. Mar. Pet. Geol. 25 (2), 153–172. http://dx.doi.org/10.1016/j.marpetgeo.2007.05.010.

Beeskow, B., Rankin, A.H., Murphy, P.J., Treloar, P.J., 2005. Mixed CH_4-CO_2fluid inclusions in quartz from the South Wales Coalfield as suitable natural calibration standards for microthermometry and Raman spectroscopy. Chem. Geol. (223), 3–15.

Bhattacharya, S., Panigrahi, M.K., Jayananda, M., 2014. Mineral thermobarometry and fluid inclusion studies on the Closepet granite, Eastern Dharwar Craton, south India: Implications to emplacement and evolution of late-stage fluid. J. Asian Earth Sci. 91, 1–18. http://dx.doi.org/10.1016/j.jseaes.2014.04004.

Bodnar, R.J., 1993. Revised equation and table for determining the freezing point depression of H_2O-NaCl solutions. Geochim. Cosmochim. Acta 57, 683–684. http://dx.doi.org/10.1016/0016-7037(93)90378-A.

Brunsgaard, H.S., Berg, R.W., Stenby, E.H., 2002. How to determine the pressure of a methane-containing gas mixture by means of two weak Raman bands, $\nu 3$ and $2\nu 2$. J. Raman Spectrosc. 33 (3), 160–164. http://dx.doi.org/10.1002/jrs.813.

Burke, E.A.J., 2001. Raman micro-spectrometry of fluid inclusions. Lithos 55 (1), 139–158. http://dx.doi.org/10.1016/S0024-4937(00)00043-8.

Chang, Y., Xu, C.H., Peter, W.R., Zhou, Z.Y., 2010. The exhumation evolution of the Micangshan-Hannan uplift since cretaceous evidences from apatite(U-Th)/He dating. Chinese J. Geophys. 53, 912–919 (in Chinese with English abstract).

Chen, Y., Zhou, Y.Q., Liu, C.Y., Yan, S.Y., Wang, Q., 2005. Quantitatively analyzing the homogenization process of CH_4-H_2O fluid inclusion by laser Raman spectroscopy. Earth Sci. Front. 12 (4), 592–596 (in Chinese with English abstract).

Chen, Y., Zhou, Y.Q., Zhang, L.P., Wu, M.H., Yan, S.Y., 2007. Discovery of CH_4-rich high-pressure fluid inclusions hosted in analcime from dongying depression, China. J. Petrol. Sci. Eng. 56 (4), 311–314. http://dx.doi.org/10.1016/j.petrol.2006.10.005.

Davis, A.R., Oliver, B.G., 1972. A vibrational-spectroscopic study of the species present in the CO_2–H_2O system. J. Solut. Chem. 1 (4), 329–339. http://dx.doi.org/10.1007/bf00715991.

Dolson, J., 2016. Using fluid inclusion data in exploration. In: Dolson, J. (Ed.), Understanding Oil and Gas Shows and Seals in the Search for Hydrocarbons. Springer, Cham, pp. 349–383. http://dx.doi.org/10.1007/978-3-319-29710-1.

Dong, D.Z., Wang, Y.M., Li, X.J., Zou, C.N., Guan, Q.N., Zhang, C.C., Huang, J.L., Wang, S.F., Wang, H.Y., Liu, H.L., Bai, W.H., Liang, F., Lin, W., Zhao, Q., Liu, D.X., Qiu, Z., 2016. Breakthrough and prospect of shale gas exploration and development in China. Nat. Gas. Ind. 36 (1), 12–26. http://dx.doi.org/10.1016/j.ngib.2016.02.002.

Dubessy, J., Buschaert, S., Lamb, W., Pironon, J., Thiéry, R., 2001. Methane-bearing aqueous fluid inclusions: Raman analysis, thermodynamic modelling and application to petroleum basins. Chem. Geol. 173 (1), 193–205. http://dx.doi.org/10.1016/s0009-2541(00)00275-8.

Fabre, D., Oksengorn, B., 1992. Pressure and density dependence of the CH_4 and N_2 Raman lines in an equimolar CH_4/N_2 gas mixture. Appl. Spect. 46 (3), 468–471. http://dx.doi.org/10.1366/0003702924125348.

Feng, G.X., Chen, S.J., 1988. Relationship between the reflectance of bitumen and vitrinite in rock. Nat. Gas. Ind. 3, 30–35 (in Chinese with English abstract).

Frezzotti, M.L., Tecce, F., Casagli, A., 2012. Raman spectroscopy for fluid inclusion analysis. J. Geochem. Explor. 112, 1–20. http://dx.doi.org/10.1016/j.gexplo.2011.09009.

Fu, D.L., Tian, T., Qin, J.Q., Yang, F., Han, Y.H., Qian, Y.F., 2018. Characterization of methane adsorption on the shales in Niutitang Formation at Dazhuba-Huijunba Oblique. J. China Coal Soc. 43 (12), 3453–3460. http://dx.doi.org/10.13225/j.cnki.jccs.2018.0389.

Gao, J., He, S., Yi, J.Z., 2015. Discovery of high density methane inclusions in Jiaoshiba shale gas field and its significance. Oil Gas Geol. 36 (3), 472–480. http://dx.doi.org/10.11743/ogg20150316.

George, S.C., Krieger, F.W., Eadington, P.J., Quezad, R.A., Greenwood, P.F., Eisenberg, L.R., Hamilton, P.J., Wilson, M.A., 1997. Geochemical comparison of oil-bearing fluid inclusions and produced oil from the Toro sandstone, Papua New Guinea. Org. Geochem. 26 (3–4), 155–173. http://dx.doi.org/10.1016/s0146-6380(97)00004-1.

George, S.C., Lisk, M., Eadington, P.J., 2004. Fluid inclusion evidence for an early, marine-sourced oil charge prior to gas-condensate migration, Bayu-1, Timor Sea, Australia. Mar. Pet. Geol. 21 (9), 1107–1128. http://dx.doi.org/10.1016/j.marpetgeo.2004.07.001.

George, S.C., Volk, H., Ahmed, M., 2007. Geochemical analysis techniques and geological applications of oil-bearing fluid inclusions, with some Australian case studies. J. Petrol. Sci. Eng. 57 (1–2), 119–138. http://dx.doi.org/10.1016/j.petrol.2005.10.010.

Guillaume, D., Teinturier, S., Dubessy, J., Pironon, J., 2003. Calibration of methane analysis by raman spectroscopy in H_2O–NaCl–CH_4 fluid inclusions. Chem. Geol. 194 (1), 41–49. http://dx.doi.org/10.1016/s009-2541(02)00270-x.

Hansen, S.B., Berg, R.W., Stenby, E.H., 2001a. High-pressure measuring cell for Raman spectroscopic studies of natural gas. Appl. Spect. 55 (1), 55–60. http://dx.doi.org/10.1366/0003702011951434.

Hansen, S.B., Berg, R.W., Stenby, E.H., 2001b. Raman spectroscopic studies of methane–ethane mixtures as a function of pressure. Appl. Spect. 55 (6), 745–749. http://dx.doi.org/10.1366/0003702011952442.

Hansen, S.B., Berg, R.W., Stenby, E.H., 2002. How to determine the pressure of a methane-containing gas mixture by means of two weak Raman bands, ν_3 and ν_2. J. Raman Spectrosc. 33 (3), 160–164. http://dx.doi.org/10.1002/jrs.813.

Horita, J., Berndt, M.E., 1999. Abiogenic methane formation and isotopic fractionation under hydrothermal conditions. Science 285 (5430), 1055–1057. http://dx.doi.org/10.1126/science.285.5430.1055.

Huang, J.L., Zou, C.N., Li, J.Z., Dong, D.Z., Wang, S.J., Wang, S.Q., Cheng, K.M., 2012. Shale gas generation and potential of the Lower Cambrian Qiongzhusi Formation in the Southern Sichuan Basin, China. Pet. Explor. Dev. 39 (1), 75–81 (in Chinese with English abstract).

Hurai, V., Marko, F., Tokarski, A.K., Świerczewska, A., Kotulová, J., Biroň, A., 2006. Fluid inclusion evidence for deep burial of the tertiary accretionary wedge of the Carpathians. Terra Nova 18 (6), 440–446. http://dx.doi.org/10.1111/j.1365-3121.2006.00710.x.

Jensensuis, J., Burruss, R.C., 1990. Hydrocarbon–water interactions during brine migration: evidence from the composition of hydrocarbon inclusions in calcite from the Danish North Sea oil fields. Geochim. Cosmochim. Acta 54 (3), 705–713. http://dx.doi.org/10.1016/0016-7037(90)90366-S.

Jiang, Y.L., Fang, L., Liu, J.D., Hu, H.J., Xu, T.W., 2016. Hydrocarbon charge history of the Paleogene reservoir in the northern Dongpu Depression, Bohai Bay Basin, China. Pet. Sci. 13 (4), 625–641. http://dx.doi.org/10.1007/s12182-016-0130-5.

Jonk, R., Parnell, J., Whitham, A., 2005. Fluid inclusion evidence for a Cretaceous–Palaeogene petroleum system, Kangerlussuaq Basin, East Greenland. Mar. Pet. Geol. 22 (3), 319–330. http://dx.doi.org/10.1016/j.marpetgeo.2005.01.002.

Kempton, R., Bourdet, J., Gong, S., Ross, A., 2017. Petroleum migration in the Bight Basin: a fluid inclusion approach to constraining source, composition and timing. APPEA J. 57 (2), 762–766. http://dx.doi.org/10.1071/aj16222.

Li, Y.F., Qu, G.S., Liu, S., Zhang, H., 2008. Structural characters and mechanism in the Micangshan and Southern Dabashan Mountains. Front. Geotect. Metal. 32 (3), 285–292. http://dx.doi.org/10.3969/j.issn.1001-1552.2008.03.004.

Liu, D.H., Dai, J.X., Xiao, X.M., Tian, H., Yang, C., Hu, A.P., Mi, J.K., Song, Z.G., 2009a. High density methane inclusions in Puguang gasfield: Discovery and a T-P genetic study. Chinese Sci Bull. 54 (24), 4714–4723. http://dx.doi.org/10.1007/s11434-009-0582-8.

Liu, D.H., Xiao, X.M., Tian, H., Wang, Y.G., Wang, Z.C., Min, Y.S., 2013. Multiple types of high density methane inclusions and their relationships with exploration and assessment of oil-cracked gas and shale gas discovered in NE Sichuan. Earth Sci. Front. 20 (1), 64–71 (in Chinese with English abstract).

Liu, D.H., Xiao, X.M., Tian, H., Yang, C., Hu, A.P., Song, Z.G., 2009b. Identification of natural gas origin using the characteristics of bitumen and fluid inclusions. Pet. Explor. Dev. 36 (3), 375–382 (in Chinese with English abstract).

Lu, W., Chou, I.M., Burruss, R.C., Song, Y.C., 2007. A unified equation for calculating methane vapor pressures in the CH_4 –H_2O system with measured Raman shifts. Geochim. Cosmochim. Acta 71 (16), 3969–3978. http://dx.doi.org/10.1016/j.gca.2007.06.004.

Morizet, Y., Paris, M., Gaillard, F., Scaillet, B., 2009. Raman quantification factor calibration for CO–CO_2 gas mixture in synthetic fluid inclusions: application to oxygen fugacity calculation in magmatic systems. Chem. Geol. (264), 58–70.

Ni, Z.Y., Wang, T.G., Li, M.J., Fang, R.H., Li, Q.M., Tao, X.H., Cao, W., 2016. An examination of the fluid inclusions of the well RP3-1 at the Halahatang Sag in Tarim Basin, northwest China: Implications for hydrocarbon charging time and fluid evolution. J. Petrol. Sci. Eng. 146, 326–339. http://dx.doi.org/10.1016/j.petrol.2016.04.038.

Okubo, S., 2005. Effects of thermal cracking of hydrocarbons on the homogenization temperature of fluid inclusions from the Niigata oil and gas fields, Japan. Appl. Geochem. 20 (2), 255–260. http://dx.doi.org/10.1016/j.apgeochem.2004.09.001.

Parnell, J., 2010. Potential of palaeofluid analysis for understanding oil charge history. Geofluids 10, 73–82. http://dx.doi.org/10.1111/j.1468-8123.2009.00268.x.

Parnell, J., Honghan, C., Middleton, D., Haggan, T., Carey, P., 2000. Significance of fibrous mineral veins in hydrocarbon migration: Fluid inclusion studies. J. Geochem. Explor. (69–70), 623–627. http://dx.doi.org/10.1016/S0375-6742(00)00040-6.

Parnell, J., Middleton, D., Chen, H., Hall, D., 2001. The use of integrated fluid inclusion studies in constraining oil charge history and reservoir compartmentation: examples from the Jeanne d'Arc Basin, offshore Newfoundland. Mar. Pet. Geol. 18 (5), 535–549. http://dx.doi.org/10.1016/S0264-8172(01)00018-6.

Roedder, E., Bodnar, R.J., 1980. Geologic pressure determinations from fluid inclusion studies. Annu. Rev. Earth Planet. Sci. 8 (1), 263–301. http://dx.doi.org/10.1146/annurev.ea.08.050180.001403.

Rogers, M.A., McAlary, J.D., Bailey, N.J.L., 1974. Significance of reservoir bitumens to thermal maturation studies, Western Canada Basin. Am. Assoc. Petrol. Geol. Bull. 58, 1806–1824. http://dx.doi.org/10.1306/83d919b6-16c7-11d7-8645000102c1865d.

Schrötter, H.W., Klöckner, H.W., 1979. Raman scattering cross-sections in gases and liquids. In: Weber, A. (Ed.), Raman Spectroscopy of Gases and Liquids. Springer-Verlag, Berlin, pp. 123–166.

Schubert, F., Diamond, L.W., Tóth, T.M., 2007. Fluid-inclusion evidence of petroleum migration through a buried metamorphic dome in the Pannonian Basin, Hungary. Chem. Geol. 244 (3–4), 357–381. http://dx.doi.org/10.1016/j.chemgeo.2007.05.019.

Seitz, J.C., Pasteris, J.D., Chou, I.M., 1993. Raman spectroscopic characterization of gas mixtures; I, Quantitative composition and pressure determination of CH_4, N_2 and their mixtures. Am. J. Sci. 293 (4), 297–321. http://dx.doi.org/10.2475/ajs.293.4.297.

Seitz, J.C., Pasteris, J.D., Chou, I.M., 1996. Raman spectroscopic characterization of gas mixtures; II, Quantitative composition and pressure determination of the CO_2-CH_4 system. Am. J. Sci. 296 (6), 577–600. http://dx.doi.org/10.2475/ajs.296.6.577.

Shang, C.J., Qiu, L.F., Li, Q., Wu, D., 2016. Characteristic of fluid inclusions in the Middle Jurassic shale gas reservoir of well Chaiye-1. J. East China Univ. Technol. (Nat. Sci.) 39 (2), 178–183 (in Chinese with English abstract).

Shepherd, T.J., Rankin, A.H., Alderton, D.H.M., 1985. A Practical Guide to Fluid Inclusion Studies. Blackie, Glasgow and New York.

Shi, H.C., Shi, X.B., 2014. Exhumation process of Middle-Upper Yangtze since Cretaceous and its tectonic significance: low-temperature thermochronology constraints. Chinese J. Geophys. 57 (8), 2608–2619. http://dx.doi.org/10.6038/cjg20140820 (in Chinese with English abstract).

Song, X., Lv, X.X., Shen, Y.Q., Guo, S., 2018. Hydrocarbon migration and accumulation history in deep reservoirs: a case study of Mesozoic sandstone gas reservoirs in the Kelasu-Yiqikelike structural belt of the Kuqa Depression, Tarim Basin. Geosci. J. 23 (1), 69–86. http://dx.doi.org/10.1007/s12303-018-0011-6.

Suchý, V., Dobeš, P., Sykorová, I., Machovič, V., Stejskal, M., Kroufek, J., Chudoba, J., Matějovsky, L., Havelcová, M., Matysová, P., 2010. Oil-bearing inclusions in vein quartz and calcite and, bitumens in veins: Testament to multiple phases of hydrocarbon migration in the Barrandian basin (lower Paleozoic), Czech Republic. Mar. Pet. Geol. 27 (1), 285–297. http://dx.doi.org/10.1016/j.marpetgeo.2009.08.017.

Tao, S., Tang, D.Z., Xu, H., Yang, F., Zhou, C.W., Li, S., 2009. Thermal history of the source rocks at high-over maturity in the Cambrian-Ordovician in Middle-Upper Yangtze. Prog. Nat. Sci. 19 (10), 1126–1133 (in Chinese with English abstract).

Tian, Y.T., Kohn, B.P., Zhu, C.Q., Xu, M., Hu, S.B., Gleadow, A.J.W., 2012. Post-orogenic evolution of the Mesozoic MicangShan Foreland Basin system, central China. Basin Res. 24 (1), 70–90. http://dx.doi.org/10.1111/j.1365-2117.2011.00516.x.

Tian, T., Zhou, S.X., Fu, D.L., Yang, F., Li, J., 2019a. Characterization and controlling factors of pores in the Lower Cambrian Niutitang shale of the Micangshan Tectonic Zone, SW China. Arab. J. Geosci. 12, 251. http://dx.doi.org/10.1007/s12517-019-4407-z.

Tian, T., Zhou, S.X., Fu, D.L., Yang, F., Li, J., 2019b. Calculation of the original abundance of organic matter at high-over maturity: A case study of the Lower Cambrian Niutitang shale in the Micangshan-Hannan Uplift, SW China. J. Petrol. Sci. Eng. 179, 645–654. http://dx.doi.org/10.1016/j.petrol.2019.04.071.

Tian, Y.T., Zhu, C.Q., Xu, M., Rao, S., Barry, P.K., Hu, S.B., 2010. Exhumation history of the Micangshan-Hannan Dome since cretaceous and its tectonic significance: evidence from Apatite Fission Track analysis. Chinese J. Geophys. 53 (4), 920–930. http://dx.doi.org/10.3969/j.issn.0001-5733.2010.04.017.

Walderhaug, O., 1994. Precipitation rates for quartz cement in sandstones determined by fluid-inclusion microthermometry and temperature-history modeling. J. Sediment. Res. 64 (2a), 324–333. http://dx.doi.org/10.2110/jsr.64.324.

Wang, L.J., Wang, Y.W., Wang, J.B., Jin, X.D., Zhu, H.P., 2000. Study of tin and copper metallogenetic fluid from Dajing deposit and its genetic significance. Acta Petrol. Sin. 16 (4), 609–614 (in Chinese with English abstract).

Wang, Y.F., Xiao, X.M., 2010. An investigation of paleo-geothermal gradients in the northeastern part of Sichuan Basin. Mar. Orig. Petrol. Geol. 15 (4), 57–61 (in Chinese with English abstract).

Wycherley, H.L., Parnell, J., Watt, G.R., Chen, H., Boyce, A.J., 2003. Indicators of hot fluid migration in sedimentary basins: evidence from the UK Atlantic Margin. Petrol. Geosci. 9 (4), 357–374.

Xi, B.B., Yu, L.J.Tenger., Jiang, H., Shen, B.J., Deng, M., 2016. Trapping pressure of fluid inclusions and its significance in shale gas reservoirs, southeastern Sichuan Basin. Petrol. Geol. Exper. 38 (4), 473–479. http://dx.doi.org/10.11781/sysydz201604473.

Xu, H.M., Liu, S., Qu, G.S., Li, Y.F., Sun, G., Liu, K., 2009. Structural characteristics and formation mechanism in the Micangshan Foreland, South China. Acta Geol. Sin. 83 (1), 81–91. http://dx.doi.org/10.1111/j.1755-6724.2009.00010.x.

Yang, Z.Q., Liu, X., Chen, J.H., 2013a. Characteristics of temperature and salinity of fluid inclusion in the East Gobi molybdenum deposit, Xinjiang. Geotech. Eng. World 4 (2), 167–176 (in Chinese with English abstract).

Yang, Z., Ratschbacher, L., Jonckheere, R., Enkelmann, E., Dong, Y.P., Shen, C.B., Wiesinger, M., Zhang, Q., 2013b. Late-stage foreland growth of China's largest orogens (Qinling, Tibet): Evidence from the Hannan-Micang crystalline massifs and the northern Sichuan Basin, central China. Lithosphere 5 (4), 420–437. http://dx.doi.org/10.1130/l260.1.

Yang, P., Ren, Z.L., Xia, B., Tian, T., Zhang, Y., Qi, K., Ren, W., 2018. Tectono-thermal evolution, hydrocarbon filling and accumulation phase of the Hari Sag, in the Yingge-Ejinaqi Basin, Inner Mongolia, Northern China. Acta Geol. Sin. (Engl. Ed.) 92 (3), 1157–1169. http://dx.doi.org/10.1111/1755-6724.13597.

Yang, P., Wu, G.H., Ren, Z.L., Zhou, R.J., Zhao, J.X., Zhang, L.P., 2020. Tectono-thermal evolution of Cambrian–Ordovician source rocks and implications for hydrocarbon generation in the eastern Tarim Basin, NW China. J. Asian Earth Sci. 104267. http://dx.doi.org/10.1016/j.jseaes.2020.104267.

Zhang, Y., Tang, H.S., Chen, Y.J., Leng, C.B., Zhao, C.H., 2014. Ore geology, fluid inclusion and isotope geochemistry of the Xunyang Hg–Sb orefield, Qinling Orogen, Central China. Geol. J. 49, 463–481. http://dx.doi.org/10.1002/gj.2560.

Zhang, N., Tian, Z.J., Leng, Y.Y., Wang, H.T., Song, F.Q., Meng, J.H., 2007. Raman characteristics of hydrocarbon and hydrocarbon inclusions. Sci. China Ser. D: Earth Sci. 50 (8), 1171–1178. http://dx.doi.org/10.1007/s11430-007-0078-9.

Zhang, N., Tian, Z.J., Mao, G.J., Wu, S.H., Liu, J.X., Tuo, Q., 2009. Ranman spectroscopic characteristics of bitumen inclusions. Geochimica 38 (2), 174–178. http://dx.doi.org/10.3321/j.issn:0379-1726.2009.02.010 (in Chinese with English abstract).

Zou, C.N., Dong, D.Z., Wang, Y.M., Li, X.J., Huang, J.L., Wang, S.F., Guan, Q.Z., Zhang, C.C., Wang, H.Y., Liu, H.L., Bai, W.H., Liang, F., Lin, W., Zhao, Q., Liu, D.X., Yang, Z., Liang, P.P., Sun, S.S., Qiu, Z., 2015. Shale gas in China: Characteristics, challenges and prospects (I). Pet. Explor. Dev. 42, 689–701. http://dx.doi.org/10.1016/S1876-3804(15)30072-0.

Zou, C.N., Dong, D.Z., Wang, Y.M., Li, X.J., Huang, J.L., Wang, S.F., Guan, Q.Z., Zhang, C.C., Wang, H.Y., Liu, H.L., Bai, W.H., Liang, F., Lin, W., Zhao, Q., Liu, D.X., Yang, Z., Liang, P.P., Sun, S.S., Qiu, Z., 2016. Shale gas in China: Characteristics, challenges and prospects (II). Pet. Explor. Dev. 43, 166–178. http://dx.doi.org/10.1016/S1876-3804(15)30022-2.